Available online at www.sciencedirect.com
SCIENCE DIRECT®
Acta Materialia 52 (2004) 1183–1192
Acta MATERIALIA
www.actamat-journals.com

Measurements and Monte Carlo simulation of grain growth in the heat-affected zone of Ti–6Al–4V welds

S. Mishra, T. DebRoy *

Department of Materials Science and Engineering, The Pennsylvania State University, University Park, PA 16802, USA

Received 16 September 2003; received in revised form 5 November 2003; accepted 5 November 2003

Abstract

Grain size and topological class distributions in the heat-affected zone (HAZ) of gas tungsten arc welded Ti–6Al–4V alloy were measured for various heat inputs in the range of 0.55–4.33 MJ m^{-1}. The evolution of grain structure and topological class distributions were also calculated using a three-dimensional Monte Carlo model utilizing thermal cycles computed from a well tested numerical heat transfer and fluid flow model. Both the experimental data and the calculated results showed that the average prior-β grain size near the fusion plane was about four to twelve times larger than the average grain size in the base plate, depending on the heat input. At locations equidistant from the fusion plane, the grains were larger in the mid-section vertical symmetry plane as compared to those at the top surface due to local variations of the thermal cycles. The normalized grain size distributions were unaffected by the local differences in the thermal cycles. It is demonstrated that the presence of a spatial gradient of temperature in the HAZ significantly impeded grain growth due to thermal pinning effect. Furthermore, the steep temperature gradients near the fusion plane did not introduce any significant texture in the grains. Both the experimental data and the calculated results indicated that the grains in the HAZ of the Ti–6Al–4V alloy were significantly smaller than the grains in the commercially pure titanium for identical welding conditions.

Keywords: Grain growth; Monte Carlo simulation; Ti–6Al–4V alloy; Heat-affected zone; Gas tungsten arc welding

1. Introduction

Titanium alloy, Ti–6Al–4V is used extensively in aerospace applications, pressure vessels, aircraft gas turbine disks, and surgical implants because of its excellent strength, toughness and corrosion resistance [1]. Welding can adversely affect the strength and toughness of this alloy because of the thermal cycles to which it is exposed [1]. High-energy input during welding causes appreciable beta (β) grain growth in the heat-affected zone (HAZ) directly adjacent to the weld fusion plane where peak temperatures range between the alloy solidus and the β-transus [1]. The resulting coarse prior-β grain size, shown in Fig. 1, significantly lowers the strength of the weld [1]. Although the grain growth behavior of commercially pure titanium during welding has been studied in details, the literature on the Ti–6Al–4V is rather scarce. A major difficulty in the characterization of the size and topological features of grains in this system arises from the impingement of a basket-weave acicular $\alpha + \beta$ on the grain boundaries during cooling [1] which makes precise identification of the grain boundaries difficult as can be seen from Fig. 1. Special time-consuming techniques are needed to clearly characterize grain structure in this alloy.

Fusion welding differs from its materials processing counterparts in many ways [2–4]. In the context of grain growth in the HAZ, two major differences merit special attention. First, the HAZ undergoes strong thermal cycles involving rapid heating and cooling. Because the kinetics of grain growth depends strongly on temperature, the evolution of grain structure in the HAZ is very different from that during isothermal processing of metals and alloys. Second, and perhaps more important, strong spatial gradients of temperature exist in the HAZ which can cause the atomic mobility to vary across large grains.

* Corresponding author. Tel.: +1-814-865-1974; fax: +1-814-865-2917.
E-mail address: debroy@psu.edu (T. DebRoy).

1359-6454/$30.00 © 2003 Acta Materialia Inc. Published by Elsevier Ltd. All rights reserved.
doi:10.1016/j.actamat.2003.11.003

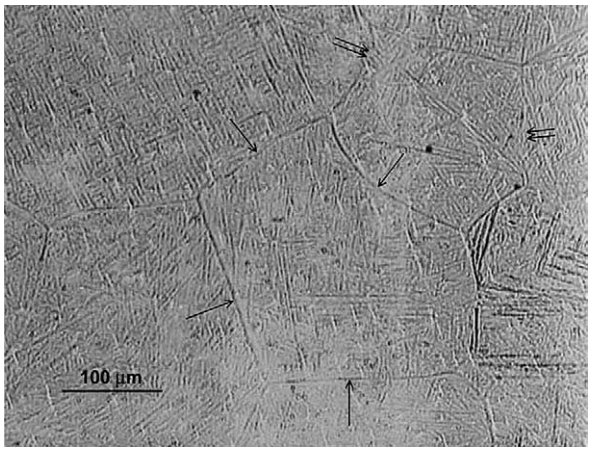

Fig. 1. Coarse prior-β grain size in the HAZ of Ti–6Al–4V alloy weld. Arrows indicate the prior β grain boundary whereas the double arrows show the impingement of the basket-weave structured acicular $\alpha + \beta$ on the grain boundaries.

Thus, in close proximity to the fusion plane where the temperature gradients are steep, different regions of a single grain may have different propensity to grow. This effect, sometimes referred to as ''thermal pinning'', cannot be conveniently translated to grain growth in isothermal systems in any straightforward manner.

The special features of fusion welding lead to several important questions at the crossroads of basic and applied sciences. How do the thermal cycles affect the grain growth behavior and the topological features of grains? What role does the spatial gradient of temperature play in the grain growth behavior? Does the temperature gradient affect the normal distribution of size which is characteristic of isothermal grain growth? Can steep temperature gradients induce texture owing to the local variations of growth in the same grain? Very little information is available in the literature to answer these basic questions. The answers to these questions, apart from being important contributions to the scientific knowledge base in fusion welding, are of great practical value since welded materials constitute more than 50% of the manufactured products in the United States [2]. Because of the complex nature of the physical processes during welding of Ti–6Al–4V alloy, a comprehensive experimental and theoretical study is needed to understand grain growth in the HAZ.

Accurate calculation of thermal cycles in the HAZ is a prerequisite to modeling grain growth. During welding, the liquid metal circulates rapidly in the weld pool and convection is often the primary mechanism of heat transfer [4]. The width of the HAZ varies with location in the weldment [4,6] and this effect can only be simulated by three-dimensional (3D) calculations of heat and fluid flow in the weldment.

The Monte Carlo (MC) technique [4–9] has been used recently for the modeling of grain growth in the HAZ. An important feature of the MC technique is that it can take into account the effect of steep temperature gradients present in the HAZ and thus incorporate ''thermal pinning'' effect. This is possible as the grains are subdivided into many discrete small units and each unit has its own mobility depending on the local temperature [6]. Furthermore, the MC technique has the inherent property of considering the evolution of grain morphology in a topologically connected network [6]. The final grain structure map obtained from MC simulations, can be used to accurately calculate the size and topological properties of the grains [10–12].

In the present study, the weld pool geometry, grain size and topological properties of grains in the HAZ have been experimentally determined for the Ti–6Al–4V alloy weldment fabricated by gas tungsten arc (GTA) welding at four heat inputs. A well-tested, 3D, heat transfer and fluid flow model [13–15] is used to calculate the temperature field, fusion zone (FZ) geometry and thermal cycles. The calculated thermal cycles are used in a MC model to simulate 3D map of grain structure in the HAZ. The FZ geometry and the MC model predictions of grain size and topological properties are then compared with the corresponding experimental results. The role of steep spatial gradient of temperature on the grain growth kinetics, topological features of grains and texture development are studied. The grain growth in the alloy is compared with that in the HAZ of commercially pure titanium welds for comparable heat inputs. The possible reasons for the differences in the grain growth behavior in HAZ of the alloy and pure metal are explored.

2. Experimental procedure

Gas tungsten arc welds were made on cylindrical samples of Ti–6Al–4V alloy. The specimens of 11.4 cm diameter were rotated at a constant speed below the fixed electrode. No preheat was used. Extra high purity helium (99.999%) was used as both the welding and shielding gas. The welding parameters used are given in Table 1. The composition of the extra low interstitial (ELI) grade alloy was (in wt%): 0.014% C, 0.11% O, 0.17% Fe, 6.0% Al, 4.2% V, less than 0.003% B, less than 0.03% Si, 0.0028% H, and less than 0.005% Y.

Optical metallography was performed on post-weld samples using conventional polishing and etching

Table 1
Welding conditions

Weld no.	Speed ($mm\,s^{-1}$)	Current (A)	Voltage (V)	Power (W)	Energy/length ($MJ\,m^{-1}$)
1	0.5	111	19.5	2165	4.33
2	1.0	111	19.2	2131	2.13
3	2.0	111	19.8	2198	1.10
4	4.0	111	19.8	2198	0.55

techniques. Different etchants were used to reveal the weld pool boundary and the grain boundaries. The weld pool boundary was revealed by using a 50% glycol and 50% hydrofluoric acid solution, and the sample was immersed in the solution for about 15 s. The etchant for revealing the grain boundaries contained 10 parts hydrofluoric acid, 10 parts nitric acid and 30 parts lactic acid. Best results were obtained by applying the etchant to the surface and swabbing continuously for 25–35 s. The mean prior-β grain size at various distances from the fusion line were measured using the lineal intercept method by placing test lines parallel to the fusion line [4] to quantitatively describe the grain size gradient in the HAZ. The number of sides and size of individual grains were also measured at different distances from the fusion line to study the evolution of topological features and the nature of the grain size distribution. Owing to a significant grain size gradient in the HAZ, different magnifications in the range 10–50× were used depending on the locations from the fusion line to ensure accurate grain size measurements. The grain size measurements were conducted using ASTM procedure on planar sections. It should be noted that these values are smaller than the "diameters" of 3D grains.

3. Mathematical modeling

3.1. Calculation of temperature field and thermal cycles

The temperature fields and thermal cycles under various welding conditions were calculated by the 3D heat transfer and fluid flow model. Detailed description of the model is given elsewhere [6,13,15,16]. Heat transfer and fluid flow calculations were performed in a 139 mm (length) × 70 mm (width) × 30 mm (thickness) domain. A $65 \times 35 \times 40$ grid system was used in the calculations. Spatially non-uniform grids were used for maximum resolution of variables. Finer grids were used near the heat source. No significant error was introduced due to heat transfer calculations in flat geometry, since the weld pool dimensions were much smaller than the dimensions of the cylindrical specimen used in the experiments. The thermophysical properties of Ti–6Al–4V alloy for calculation of the heat transfer and fluid flow are given in Table 2. From the calculated temperature field, the FZ geometry was determined by the solidus temperature (1878 K) of the alloy. The HAZ geometry cannot be predicted exactly since the starting temperatures for the annealing and recrystallization of α-phase are not known precisely. However, the β-phase containing region (α partially or fully transformed to β), which is the main area of concern for coarse grain size in the HAZ, can be predicted from the computed temperature field. This region exists between the α/β transition isotherm (1248 K) and the isotherm for the solidus temperature (1878 K). This β-phase containing region was denoted as the HAZ [4] and its width was predicted from the calculated result. Furthermore, the calculated thermal cycles at different locations in the HAZ, at varying temperatures ranging from the α/β transition temperature to the peak temperature during heating followed by cooling from the peak temperature to the β/α transition temperature, were used for modeling the growth of β-grains. It should be noted that the model considers temperature gradients in all the three directions.

Table 2
Data used for the calculation of velocity and temperature fields

Physical property	Value	Reference
Liquidus temperature (K)	1928	[17]
Solidus temperature (K)	1878	[17]
Density of liquid metal ($kg\,m^{-3}$)	4000[a]	–
Viscosity of liquid ($kg\,m^{-1}\,s^{-1}$)	4.9×10^{-3}[a]	–
Thermal conductivity of solid ($J\,m^{-1}\,s^{-1}\,K^{-1}$)	20	[17]
Thermal conductivity of liquid ($J\,m^{-1}\,s^{-1}\,K^{-1}$)	20[b]	–
Specific heat of solid ($J\,kg^{-1}\,K^{-1}$)	610	[18]
Specific heat of liquid ($J\,kg^{-1}\,K^{-1}$)	700[a]	–
Temperature coefficient of surface tension ($N\,m^{-1}\,K^{-1}$)	-0.28×10^{-3}[a]	–
Thermal expansion coefficient (K^{-1})	1.1×10^{-5}	[17]

[a] Values for commercially pure titanium were used [4].
[b] Estimated value was used since data are not generally available in the literature.

3.2. Grain growth kinetics

The application of the MC technique to model grain growth in the HAZ of welds has been reported in the literature [4–9]. Only the modifications and salient features pertinent to the specific problem are described here. The relation between the average grain size, L, and the initial average grain size, L', valid for the simulation of grain growth in the entire HAZ, can be written as

$$L = L' + K_1 \times \lambda \times (t_{MCS})^{n_1}, \quad (1)$$

where λ is the discrete grid point spacing in the MC technique, t_{MCS} is the MC simulation time, and K_1 and n_1 are model constants. Eq. (1) represents the intrinsic grain growth kinetics of the MC model where L and t_{MCS} are dimensionless quantities. However, in the dimensionless growth kinetics of MC simulation, the initial average grain size, L', has no relation to the actual initial average grain size, L_0, of the real material under consideration. The variable L' is set equal to the grid spacing, λ, for MC simulation. Thus, Eq. (1) becomes

$$L = \lambda + K_1 \times \lambda \times (t_{MCS})^{n_1}. \quad (2)$$

The grain growth kinetics obtained from the MC technique need to consider material properties and temperature–time history. To simulate grain growth of a

specific material under specified thermal conditions, a relation needs to be established between t_{MCS} and the given conditions. The experimental data based (EDB) model, proposed by Gao et al. [7], has been adopted in this study. They represented the data obtained from isothermal grain growth experiments by the following relation [7]:

$$L^n - L_0^n = Kt \exp\left(-\frac{Q}{RT}\right) \tag{3}$$

where L is the average grain size at a given time, L_0 is the initial average grain size, T is the temperature, t is the time, R is the universal gas constant, n is the grain growth exponent, K is the pre-exponential factor, and Q is the grain growth activation energy. Combining Eqs. (2) and (3) and integrating over an entire thermal cycle, the modified relation for the EDB model becomes

$$t_{MCS} = \left[\frac{1}{K_1\lambda}\left\{K\sum_i\left(\Delta t_i \exp\left(-\frac{Q}{RT_i}\right)\right) + L_0^n\right\}^{\frac{1}{n}} - \frac{1}{K_1}\right]^{\frac{1}{n_1}}, \tag{4}$$

where T_i is the mean temperature in a small time interval of duration Δt_i. Thus, at any monitoring location where the temperature is known as a function of time, t_{MCS} can be related to real time ($t = \sum \Delta t_i$) using Eq. (4). Higher the temperature and longer the time for grain growth at a site, the higher is the value of t_{MCS} obtained from Eq. (4). Thus, sites closer to the fusion plane having stronger thermal cycles, get higher values of t_{MCS} assigned to them. The isothermal experimental data required by this model are taken from Gil et al. [19]. They measured various grain size parameters for grain growth at different temperatures in the β-phase region of the alloy. The grain growth exponent, n, the pre-exponential factor, K, and the grain growth activation energy, Q, were obtained as constants. The values of these parameters are given in Table 3.

3.3. The MC simulation step and site selection probability

In the MC technique, the choice of grid point for updating the grain orientation number is random and, as a consequence, the probability to select each grid point is the same. However, grains must grow at faster rates in regions of higher temperatures in the HAZ and this fact must be included in the calculation scheme. In the current scheme, the thermal cycle in the weld HAZ which is a function of distance from the fusion plane, is represented by gradient of t_{MCS} which, in turn, is incorporated in the simulation by visiting each site with a probability, p [8]:

$$p = t_{MCS}/t_{MCSMAX} \tag{5}$$

where, t_{MCS} is the computed MC simulation time at any site and t_{MCSMAX} is the maximum MC simulation time in the entire simulation domain. Thus, locations with higher t_{MCS} are updated more frequently.

Table 3
The isothermal experimental data required by the EDB model [19]

Grain growth activation energy, Q (J mol^{-1})	1.7×10^5
Experimental grain growth exponent, n	1.84
Pre-exponential factor, K	3.01×10^{-2}

3.4. Numerical scheme

In the present study, 3D simulations were carried out in a cubic lattice system. The simulation domain included only one of the two work pieces being joined since the other piece is a mirror image of the domain considered. More details about the computational domain are given in [4]. The grid spacing, λ, was set equal to the experimentally measured initial average grain size, i.e. 30 μm. The grid system used to represent the calculation varied with heat input because of the different sizes of the weld obtained. For instance, for a heat input of 2.13 MJ/m, the grid system used was $100 \times 350 \times 200$, which corresponds to a domain size of $(100 \times 30$ μm$) \times (350 \times 30$ μm$) \times (200 \times 30$ μm$) = 3.0 \times 10.5 \times 6.0$ mm^3, taken at the center of the weld.

3.5. Distribution of t_{MCS} and the probability

The temperature–time history at each site was incorporated into the model as follows. The values of K_1 and n_1 were calculated using Eq. (1). A plot of $\ln((L - L')/\lambda)$ versus $\ln(t_{MCS})$ was constructed for a temperature of 1563 K, which is the median temperature of the solidus (1878 K) and the β-transus (1248 K) [17] temperatures for the alloy. The values of K_1 and n_1 were determined to be 0.64 ± 0.02 and 0.50 ± 0.01, respectively, from the intercept and the slope of the linear fit to the calculated data. The other material dependent constants i.e. n, K and Q, were obtained from isothermal experimental data and are given in Table 3. The variation in the activation energy, Q, due to possible compositional inhomogeneity of the β-grains in the HAZ was ignored. Consequently, the t_{MCS} values at each site were calculated from Eq. (4) by incorporating the appropriate thermal history into the equation. Using the spatial distribution of t_{MCS} in the domain the corresponding distribution of site-selection probability, p, was obtained from Eq. (5). To obtain a realistic grain structure, more than 200 iterations were conducted in all the cases.

3.6. Calculation of grain size and topological features

Finally, after getting the calculated grain structure map in the HAZ from the MC simulations, different

modules were created in the code to calculate the size and topological features of the grains in the map.

4. Results and discussion

4.1. Weld geometry

The calculated FZ geometry, determined by the solidus temperature (1878 K) of the alloy, is compared with the corresponding experimental result for a heat input of 2.13 MJ m^{-1} in Fig. 2. The calculated FZ geometry matches fairly well with the experimental result confirming the reliability of the calculated temperature field. Since the starting temperatures for the annealing and recrystallization of α-phase are not known precisely, the geometry of the HAZ cannot be exactly predicted. However, the β-phase containing region (α partially or fully transformed to β) in the HAZ, or the near-HAZ region, which is the main area of concern for the coarse grain size [20], can be predicted from the computed temperature field. This region exists between the α/β transition isotherm (1248 K) and the isotherm for the solidus temperature (1878 K). This β-phase containing region is denoted as the HAZ [4] and its width is predicted from the calculated temperature profile shown in Fig. 2.

Fig. 2 shows that the weld pool is wide and shallow. This geometry results from convective transport of heat from the middle to the periphery of the weld pool surface consistent with negative temperature coefficient of surface tension ($d\gamma/dT$) of the alloy. The relative importance of convection and conduction in the overall transport of heat in the weld pool can be assessed from the value of the Peclet number, *Pe*, which is given by

$$Pe = \frac{u\rho C_p L}{k} \tag{6}$$

where u is the velocity, ρ is the density, C_p is the specific heat at constant pressure, L is the characteristic length, and k is the thermal conductivity of the melt. When *Pe* is large, which in physical terms means large melt velocity, large weld-pool, and poor thermal conductivity, the convective effects, i.e. the weld pool velocities, markedly affect the heat transfer. In the Ti–6Al–4V alloy welds, typical velocity in the pool is 0.15 m s^{-1}, the density is 4000 kg m^{-3}, the specific heat is 700 J kg^{-1} K^{-1}, the weld depth is 0.002 m, and the thermal conductivity is 20 W m^{-1} K^{-1}. The corresponding value of *Pe* is found to be 42 which is much larger than unity. This value of *Pe* indicates that heat is transported mainly by convection in the weld pool. Therefore, accurate calculations of temperature fields can only be done by considering convective heat transport.

Fig. 2 shows that the width of the HAZ at various locations is different. At the top surface, the width is smaller than that below the weld pool. This behavior is due to the local variation of thermal cycles during welding which causes comparatively lower temperatures and consequently smaller spread of thermal gradient on the top surface than that below the heat source in the interior of the specimen.

The experimental and calculated depth and half-width of the weld pool (FZ) for the four heat inputs considered in the present study are listed in Table 4. The calculated results match fairly well with the experiments

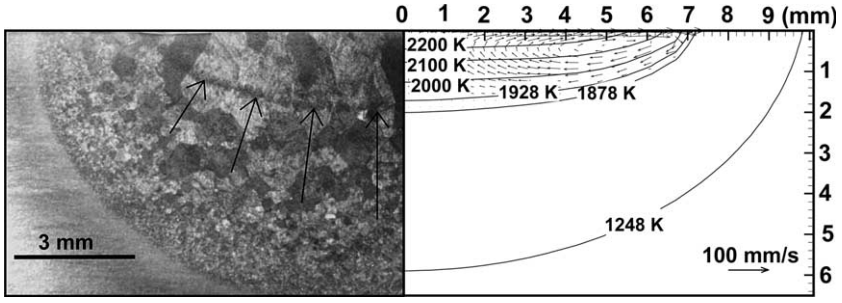

Fig. 2. Comparison of the calculated and experimental geometries for a GTA weld in Ti–6Al–4V alloy. Heat input is 2.13 MJ m^{-1}. The arrows show the location of the fusion zone boundary in the micrograph.

Table 4
Comparison of the calculated weld pool dimensions with the experimental results

Weld no.	Energy/length (MJ m^{-1})	Depth (mm)		Half-width (mm)	
		Experimental	Calculated	Experimental	Calculated
1	4.33	2.7	2.9	10.1	9.9
2	2.13	2.0	2.0	6.3	7.2
3	1.10	1.5	1.6	6.0	5.9
4	0.55	1.1	1.1	4.8	4.7

indicating the reliability of the numerical model used. Both the experimental and theoretical results show that the depth and the width decrease significantly with decrease in heat input.

4.2. Grain size distribution in the HAZ

The variations of the mean grain size with distance from the weld center line, on the mid-section vertical symmetry plane, are plotted in Fig. 3 for the four heat inputs. In all the cases the maximum average grain size is observed near the fusion plane. For a heat input of 4.33 MJ m^{-1} the average grain size is 12 times the initial average grain size of 30 μm. The extent of grain growth i.e. the distance over which large grain size is found, is significantly large for a heat input of 4.33 MJ m^{-1}. However, when using lower heat input, say 0.55 MJ m^{-1}, the average grain size near the fusion plane is only four times the initial average grain size and the extent of growth is almost one-third of that for 4.33 MJ m^{-1}, as seen in Fig. 3. These results show that the heat input strongly affects grain growth and that the large grain size can be avoided in the HAZ by using smaller energy input when possible. Furthermore, Fig. 3 shows that the calculated average grain size agrees well with the experimentally measured values. This agreement indicates that the MC grain growth model, utilizing the thermal cycles obtained from the numerical heat transfer and fluid flow model, can effectively simulate the effect of heat input on grain growth in the HAZ.

To study the effect of the local variation of thermal cycles on grain growth in the HAZ, the variation of the mean grain size with distance from the fusion plane is plotted in Fig. 4 for the mid-section vertical symmetry plane (line CD) and the top surface (line AB) for a heat input of 2.13 MJ m^{-1}. The grain growth is more pronounced along the mid-section vertical symmetry plane

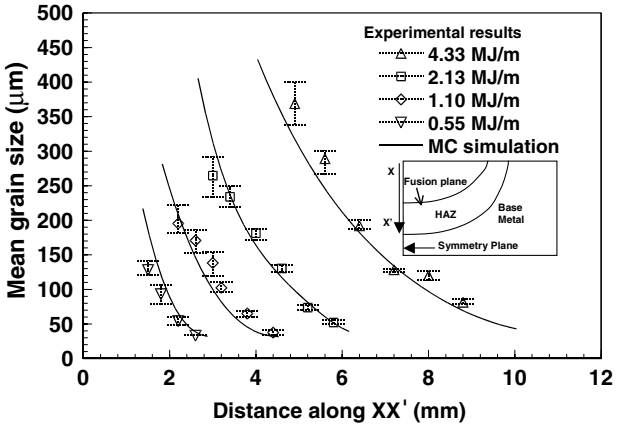

Fig. 3. Comparison of the calculated and experimental mean grain size at various locations on the mid-section vertical symmetry plane of welds (along XX′).

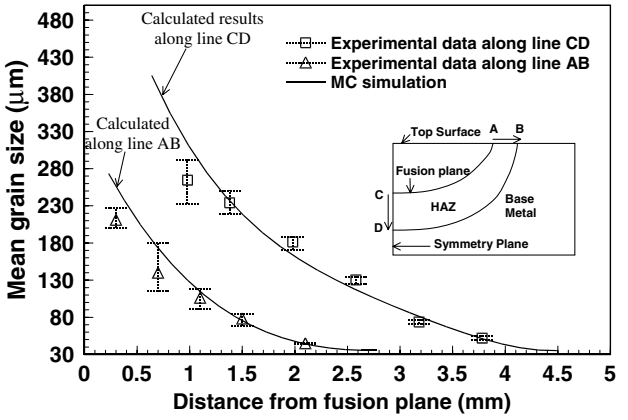

Fig. 4. Comparison of the mean grain size at different distances from the fusion plane on the mid-section vertical symmetry plane (line CD) and the top surface (line AB) for a heat input of 2.13 MJ m^{-1}.

because at any given distance from the fusion plane, the thermal cycle in this plane is stronger than that on the top surface. The difference in the thermal cycles can be observed in Fig. 5 where the thermal cycles at 1 mm from the fusion plane are presented for the two surfaces. The peak temperature and the area under the thermal cycle at the top surface are lower than the corresponding values of these parameters at the mid-section vertical symmetry plane.

An important feature associated with the variation of thermal cycles in the HAZ is the presence of steep temperature gradients near the fusion plane. The presence of a steep temperature gradient can cause the atomic mobility to vary across a large grain. This variation causes "thermal pinning" of grain growth in the HAZ of welds [5,8,21,22]. Fig. 6 illustrates this effect. The solid curve shows the grain growth kinetics at a distance of 1 mm from the fusion plane on the mid-

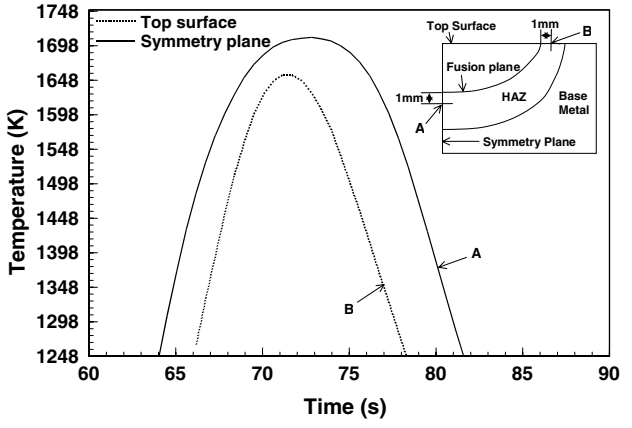

Fig. 5. Temperature fields at a distance of 1 mm from the fusion plane on the top surface and the mid-section vertical symmetry plane for a heat input of 2.13 MJ m^{-1}. The time scale is calculated by dividing the x-distance by welding speed and time = 0 is arbitrarily set when the heat source is located at $x = 0$.

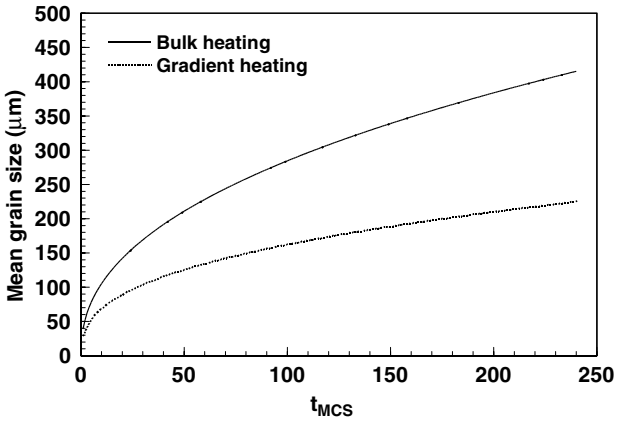

Fig. 6. The kinetics of grain growth at a distance of 1 mm from the fusion plane on the mid-section vertical symmetry plane. The dotted curve represents the kinetics under steep temperature gradients normally observed in the HAZ (gradient heating). The solid line curve is the kinetics obtained when the bulk material is subjected to a uniform thermal cycle observed at 1 mm from the fusion plane on the mid-section vertical symmetry plane (bulk heating). The rate of growth is much faster in the latter case.

section vertical symmetry plane when the entire calculation domain was subjected to a single thermal cycle observed at that location in real welds (bulk heating). The dotted curve shows the grain growth kinetics at the same location under normal welding conditions with steep temperature gradients. It is observed that the growth rate is much higher during bulk heating.

Back scattered electron diffraction (orientation imaging microscopy) and X-ray diffraction techniques were used to examine whether the presence of steep temperature gradients across large grains can induce texture in the HAZ. Analysis was done at locations close to the FZ where very steep temperature gradients exist, and further away from the HAZ in the base metal where randomly oriented equiaxed grains were expected. There was no significant texture seen in the grains at both the locations showing that the steep temperature gradients did not cause the grains to have any preferred orientation.

To study the influence of thermal cycles on the grain size distributions, the frequency versus normalized grain size plots are drawn in Figs. 7(a) and (b) and 8. Fig. 7(a) shows the distributions at a distance of 1 mm from the fusion plane on the top surface and the mid-section vertical symmetry plane for a heat input of 2.13 MJ m^{-1}. Fig. 7(b) shows the grain size distributions at the same distance from the fusion plane and on the same surface for two different heat inputs, and Fig. 8 compares the grain size distribution at 1 mm from the fusion plane on the mid-section vertical symmetry plane for a heat input of 2.13 MJ m^{-1} with that obtained under bulk heating conditions when the entire sample was subjected to the thermal cycle observed at this location. An important

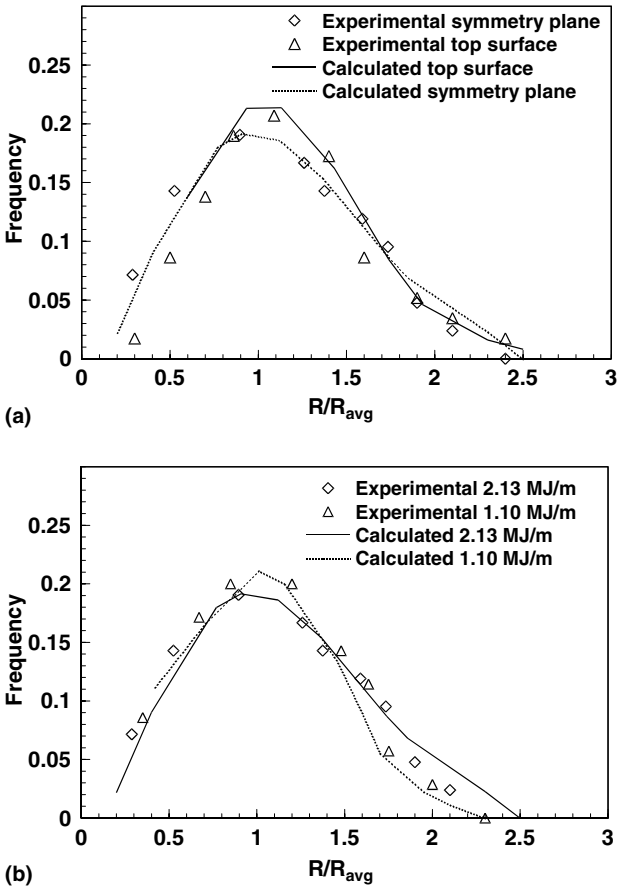

Fig. 7. (a) Experimental and calculated grain size distributions at 1 mm from the fusion plane on the top surface and the mid-section vertical symmetry plane for a heat input of 2.13 MJ m^{-1}. (b) Experimental and calculated grain size distributions at 1mm from the fusion plane on the mid-section vertical symmetry plane for heat inputs of 1.10 and 2.13 MJ m^{-1}.

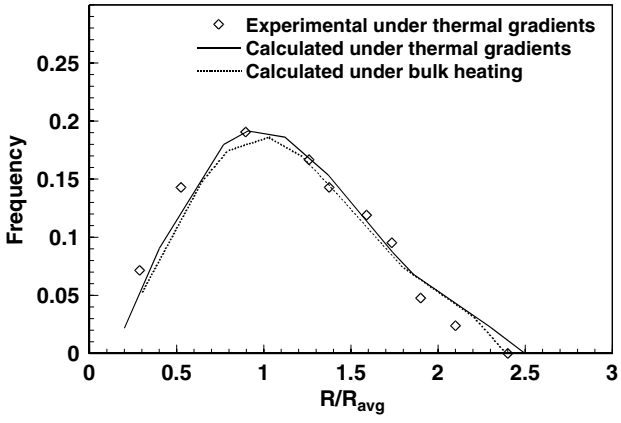

Fig. 8. Grain size distribution at 1 mm from the fusion plane on the mid-section vertical symmetry plane for a heat input of 2.13 MJ m^{-1} compared with that under bulk heating conditions when the entire sample was subjected to a single thermal cycle observed at the above location.

feature of these plots is that all the distributions are fairly identical i.e. unaffected by the difference in thermal cycles. These results indicate the time invariance of grain

size distributions during normal grain growth in different materials [10,12,23]. This behavior can be explained from the fact that any thermal cycle in the HAZ can be visualized as a collection of a large number of discreet isothermal steps applied for different times. The grain size distribution under different thermal cycles thus behaves in a similar manner as that under different isothermal conditions for different times, i.e. remains invariant. All the calculated and experimental results show asymmetric peaks in the range of R/R_{avg} between 0.5 and 1.5, and the maximum grain size is about 2.5 times the average grain size at all the locations, which indicates microstructural homogeneity of grain growth in the HAZ of the alloy even under steep thermal gradients.

4.3. Topological properties of grains in the HAZ

To understand the relationship between the size and topology of grains under intense thermal cycles in the weld HAZ, the average grain size for each edge class is plotted against the edge class number (number of edges) in Fig. 9. The plot shows the experimental and calculated data at 2 mm from the fusion plane on the mid-section vertical symmetry plane for two heat inputs. A linear relationship is observed in both the cases showing that grains with larger number of sides (lower grain boundary length per unit area) grow more. Good agreement is observed between the calculated and the experimental results indicating that the MC model can accurately predict both size and topological features of grains in the HAZ of the alloy.

The average perimeter per grain at different locations on the mid-section vertical symmetry plane is plotted in Fig. 10. The bars represent experimental data, the solid dots represent calculated data and the dashed line represents exponential fit to the calculated data. The average perimeter per grain decreases for successive locations away from the fusion plane owing to the smaller average grain size due to weaker thermal cycles. The fit to the calculated data shows that the variation of average perimeter per grain follows the same trend as the variation of mean grain size. The calculated results match fairly well with the experimental data indicating the effectiveness of the present MC model.

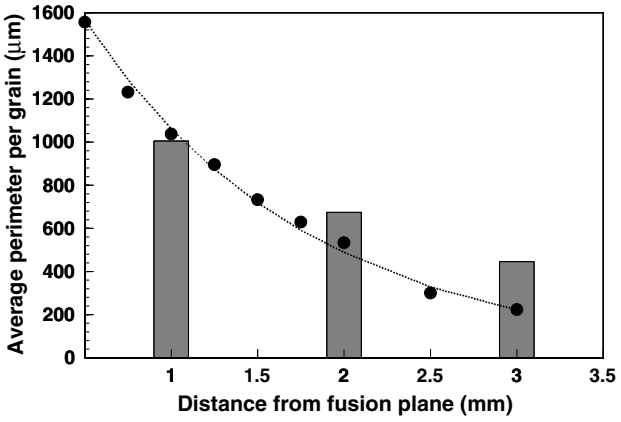

Fig. 10. Comparison of the experimental (bars) and calculated (solid dots) average perimeter per grain at different distances from the fusion plane on the mid-section vertical symmetry plane for a heat input of 2.13 MJ m^{-1}.

4.4. Comparison of grain growth in titanium and its alloy

The mean grain size at different distances from the fusion plane in commercially pure titanium [4] and Ti–6Al–4V alloy welds are compared for roughly similar heat inputs in Fig. 11. The results are for the top surface

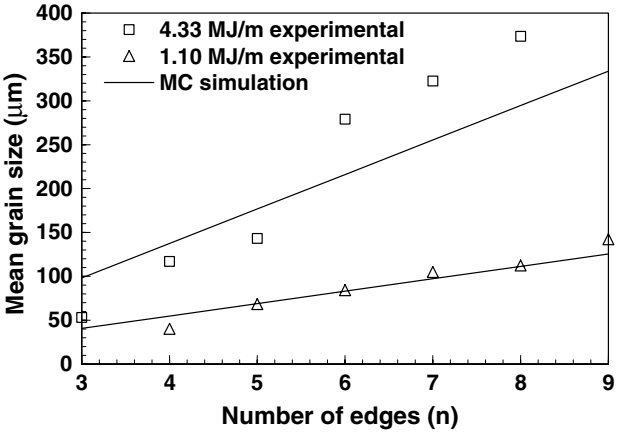

Fig. 9. Mean grain size versus number of edges at 2 mm from the fusion plane on the mid-section vertical symmetry plane for the two heat inputs. The symbols represent the experimental data while the solid lines are the linear fit to the calculated results for the two heat inputs.

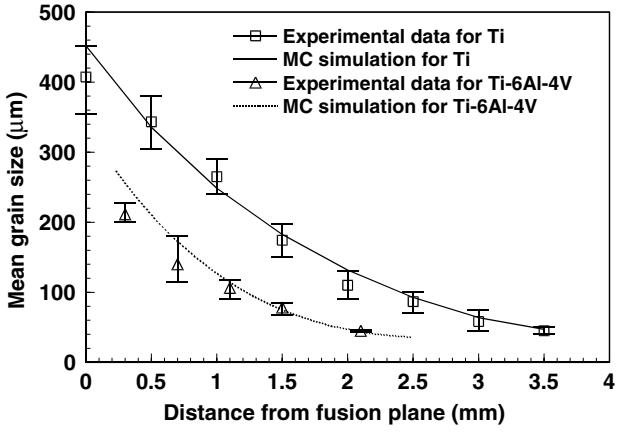

Fig. 11. Comparison of the experimental and calculated mean grain size at different distances from the fusion plane on the top surface of the welds in commercially pure titanium (heat input: 2.0 MJ m^{-1}) [4] and ELI grade Ti–6Al–4V alloy (heat input: 2.1 MJ m^{-1}).

of the welds. It is observed, that the average grain size at all locations of the alloy weld is approximately half of that in the commercially pure titanium weld. The width of the HAZ of the alloy weld is also almost half of that of the commercially pure titanium weld.

The HAZ size in the two materials differs considerably. Commercially pure titanium has a solidus temperature of 1941 K [4] and β-transus of 1158 K [4], as against the solidus temperature of 1878 K and β-transus of 1248 K for the alloy. The width of the HAZ in the present study is assumed to be enclosed by two isotherms, i.e., the β-transus and solidus temperature. Thus, in commercially pure titanium, the thermal cycles in the HAZ are spread over a temperature range between 1158 and 1941 K, i.e. a temperature range of 783 K. In contrast, in the HAZ of the alloy, β is stable between 1248 and 1878 K which represents a 630 K span. Therefore, the alloy will have significantly lower HAZ width as is seen in the present study.

The solidus temperature of the commercially pure titanium (1941 K) is about 63 K more than that of the alloy (1878 K). Therefore, at any given distance from the fusion plane (solidus temperature) the peak temperature is higher in the commercially pure titanium than that in the alloy. Higher temperatures favor grain growth. So, at any given distance from the fusion plane, the grains are larger in the commercially pure titanium than in the alloy. Furthermore, the β-transus for the alloy is about 90 K higher than that of the commercially pure titanium. It is known that when the titanium or its alloy is annealed below the β-transus, α-phase forms and prevents further β-grain growth [20]. Since the β-transus of the alloy is significantly higher than that of the commercially pure titanium, β will transform to α at a higher temperature and prevent further grain growth resulting in smaller grain size. In addition, in the alloy the newly formed α phase forms a basket-weave structure with the retained-β, which impinges on the grain boundaries impeding grain boundary motion, as illustrated in Fig. 1 by the double arrows. In addition, the activation energy of grain growth in pure titanium [4], 102 kJ/mol, is smaller than that in the alloy [19], 170 kJ/mol. Thus, the kinetics of grain growth is faster in pure titanium.

The curves in Fig. 11 represent the calculated data. It can be seen that the calculated results match fairly well with the experimental results for both the commercially pure titanium [4] and the alloy. This excellent correlation gives confidence in predicting grain growth in the HAZ of titanium and its alloys using the MC technique.

5. Conclusions

The FZ geometry and grain structure in the HAZ of Ti–6Al–4V alloy GTA welds were studied experimentally and theoretically. The grain growth in the HAZ of Ti–6Al–4V alloy was compared with that in the commercially pure titanium. The following are the main conclusions:

1. The experimentally determined FZ geometry agreed well with the corresponding values calculated from a 3D heat transfer and fluid flow model for various values of heat input. The high values of computed Peclet number for heat transfer indicated the need for considering convective heat transfer in calculating both the weld pool geometry and the thermal cycles in the Ti–6Al–4V weldments.
2. The experimental data as well as the calculated results showed that the average grain size near the fusion plane was about four to twelve times larger than that in the base plate depending on the heat input used. The extent of grain growth in the HAZ was strongly dependent on the heat input.
3. The computed grain size for various heat inputs agreed well with the corresponding experimental data. The results showed that at locations equidistant from the fusion plane the mean grain size was larger in the mid-section vertical symmetry plane than at the top surface. This behavior is consistent with the local variations of thermal cycles at locations equidistant from the fusion plane. Furthermore, the width of the HAZ in the mid-section vertical symmetry plane was higher than that near the top surface.
4. The average grain size in the weld HAZ was significantly smaller than that would be obtained in a bulk material experiencing the same thermal cycle but without any spatial temperature gradient. The thermal pinning effect resulting from the steep temperature gradient in the HAZ significantly impedes grain growth kinetics. Steep temperature gradients near the fusion plane did not introduce any significant texture in the grains.
5. The grain size distributions showed asymmetric peaks between R/R_{avg} equal to 0.5 and 1.5, and had a maximum value of about 2.5. The grain size distributions were found to be identical for different locations in the HAZ. The average grain size for each edge class was proportional to the edge class number in the HAZ.
6. Both the calculated results and the experimental data showed that for identical welding conditions, the grain size in the HAZ of the alloy was significantly smaller than that in the commercially pure titanium.

Acknowledgements

This research was supported by a grant from the US Department of Energy, Office of Basic Energy Sciences, Division of Materials Sciences, under grant number DE-FGO2-01ER45900. The authors thank Drs. Todd A. Palmer and John W. Elmer of LLNL for providing

welded samples and for their interest in the research. Valuable critical comments from Dr. L.Q. Chen during the preparation of the manuscript are appreciated. The authors thank Mr. Wei Zhang, Mrs. Xiuli He, Mr. Amit Kumar, Dr. Cheolhee Kim and Dr. Amitava De for their comments on various drafts of this manuscript.

References

[1] Donachie Jr MJ. Titanium: A technical guide. 2nd ed. Materials Park (OH): ASM International; 2000.
[2] DebRoy T, David SA. Science 1992;257:497.
[3] DebRoy T, David SA. Rev Modern Phys 1995;67:85.
[4] Yang Z, Sista S, Elmer JW, DebRoy T. Acta Mater 2000;48:4813.
[5] Sista S, Yang Z, DebRoy T. Metall Mater Trans 2000;B31:529.
[6] Yang Z, Elmer JW, Wong J, DebRoy T. Weld J 2000;79:97s.
[7] Gao J, Thompson RG, Cao Y. In: Smartt HB, Johnson JA, David SA, editors. Trends in welding research. Materials Park (OH): ASM International; 1996. p. 199.
[8] Radhakrishnan B, Zacharia T. Metall Mater Trans A 1995;26:2123.
[9] Wilson AL, Martukanitz RP, Howell PR. In: Vitek JM, David SA, Johnson JA, Smartt HB, DebRoy T, editors. Trends in welding research. Materials Park (OH): ASM International; 1998. p. 161.
[10] Srolovitz DJ, Anderson MP, Sahni PS, Grest GS. Acta Metall 1984;32:793.
[11] Saito Y, Enomoto M. ISIJ Int 1992;32:267.
[12] Sista S, DebRoy T. Metall Mater Trans B 2001;32B:1195.
[13] Mundra K, DebRoy T, Kelkar K. Numerical Heat Transfer 1996;29:115.
[14] Pitscheneder W, DebRoy T, Mundra K, Ebner R. Weld J 1996;75:71s.
[15] Zhang W, Roy GG, Elmer JW, DebRoy T. J Appl Phys 2003;93:3022.
[16] Yang Z, DebRoy T. Metall Trans B 1999;30:483.
[17] Boyer R, Welsch G, Collings EW, editors. Materials properties handbook: titanium alloys. Materials Park (OH): ASM International; 1994.
[18] Brandes EA, Brook GB, editors. Smithells light metals handbook. Oxford: Butterworth-Heinemann; 1998.
[19] Gil FJ, Tarin P, Planell JA. In: Froes FH, Captan I, editors. Titanium'92, science and technology. Warrendale: TMS; 1993. p. 777.
[20] Olson DL, Siewert TA, Liu S, Edwards GR. In: Welding, brazing and soldering, welding handbook, vol. 6. Materials Park (OH): ASM International; 1995.
[21] Easterling K. In: Introduction to the physical metallurgy of welding. London: Butterworths; 1983. p. 134.
[22] Alberry PJ, Jones WKC. Met Technol 1977;4:557.
[23] Hu H. Can Metal Q 1974;13:275.